PLEASE CITE THIS ARTICLE AS DOI: 10.1063/5.0087850

Accurate Time Zero Determination in an Ultrafast Transmission Electron Microscope without Energy Filter

Pavel K. Olshin, Jonathan M. Voss, Marcel Drabbels, and Ulrich J. Lorenz*

Ecole Polytechnique Fédérale de Lausanne (EPFL), Laboratory of Molecular Nanodynamics, CH-1015 Lausanne, Switzerland

* To whom correspondence should be addressed. E-mail: ulrich.lorenz@epfl.ch

Abstract

In ultrafast transmission electron microscopy, time zero can be accurately determined by making use of the photon-induced near-field electron microscopy (PINEM) effect, which causes electrons interacting with the near fields of a nanoparticle to coherently gain or lose energy in multiples of the photon energy when the laser pump and electron probe pulse overlap in time. If the instrument is not equipped with an energy filter, which is required to observe the PINEM effect, the response of a sample is frequently monitored instead. However, the gradual or delayed onset of this response can render an accurate measurement challenging. Here, we demonstrate a simple and accurate method for determining time zero without energy filter that is based on the observation that the outline of a nanoparticle blurs when the electron and laser pulse overlap in time. We show that this phenomenon arises from the PINEM effect, which causes some electrons to gain a large energy spread, thus blurring the image due to the chromatic aberration of the imaging system. This effect can also be used to characterize the instrument response and determine the laser polarization *in situ*. Furthermore, it may find application for mapping out the near fields of a nanoparticle without the help of an energy filter.

Ultrafast transmission electron microscopy[1,2] has become a powerful technique for directly visualizing nanoscale dynamics with ultrafast time resolution. Its popularity is underlined by the wide variety of phenomena that have been studied, including the mechanical oscillations of nanostructures,[3,4] the propagation of acoustic phonons,[5,6] ultrafast phase transitions,[7,8] and chemical transformations.[9–11] It has also given rise to new approaches for coherently manipulating free electron wavepackets.[12–16] In all of these experiments, it is crucial to accurately determine time zero, *i.e.* the time origin of the experiment at which the laser pump and electron probe pulse overlap in time at the sample. The methods for finding time zero typically employed in laser pump-electron probe experiments broadly fall into two categories. The first monitors a fast sample response at time zero, which ideally should resemble a step function. Suitable processes include the ultrafast lattice dynamics in 2D materials,[17,18] the expansion of a solid under impulsive laser heating,[19,20] the excitation of acoustic waves in an ordered solid,[6,21,22] and the magnetization dynamics observed in Lorentz microscopy.[23,24] The so-called transient electric field effect[25] is frequently employed as well, which arises when the sample is ionized at high pump laser intensity. The cloud of emitted electrons deflects or distorts the ultrafast electron pulse, which can be observed either in real space or in diffraction.[26–30] A common drawback of these methods is that the onset of the sample response may be slow or even delayed. For example, the deflection of the electron beam due to the transient electric field effect sets in gradually as the cloud of emitted electrons expands and begins to undergo complex motions.[26] Clearly, the sample response is not a step function in this instance, which renders an accurate determination of time zero more difficult.

Such complications are avoided in experiments that instead monitor electron-photon interactions, which are only present when the electron and laser pulse overlap in time. The ponderomotive interaction, which is quadratic in the electric field, accelerates electrons in the direction of lower fields. A tightly focused laser beam will therefore burn a hole into the electron cloud at time zero.[31–34] However, since the ponderomotive interaction is weak, this method requires high pulse energies (typically hundreds of microjoules), which may be impractical to use in an ultrafast transmission electron microscope. In contrast, the linear interaction of the electrons with the light field that gives rise to the PINEM effect can be observed at much lower laser intensities. It causes electrons traveling through the optical near fields of a nanostructure to gain or lose energy in multiples of the photon energy.[12,35,36] In some geometries, the energy spread can even reach up to hundreds of electron volts.[16,36,37] By monitoring the appearance

of sidebands in the electron energy loss spectrum (EELS) or the depletion of the zero-loss peak, time zero as well as the instrument response can be accurately determined.[14,38–42] This measurement, however, requires an energy analyzer, a costly piece of equipment that is not available on all instruments.

Here, we demonstrate that time zero can be accurately determined without energy filter by monitoring the width of the boundary of a nanoparticle, which increases when the electron and laser pulse overlap in time. Our experiments provide evidence that this phenomenon results from the PINEM effect, which causes electrons interacting with the near fields of the nanoparticle to acquire a large energy spread, which couples to the chromatic aberration of the imaging system and thus blurs the particle outline. This conclusion is supported by the pronounced angular dependence of the blurring, which closely resembles that of the PINEM effect. Moreover, we demonstrate the magnitude of the blurring is consistent with the energy spread that the electrons have acquired.

Experiments are performed with a modified JEOL 2200FS transmission electron microscope.[43] Femtosecond time-resolved experiments are performed at 100 kHz repetition rate. The sample is illuminated at close to normal incidence with femtosecond laser pulses (515 nm, 200 fs), with the laser beam focused to a spot size of 24±1 µm FWHM in the sample plane, as measured *in situ* with a knife edge scan. Time-delayed femtosecond electron pulses are generated by illuminating the emitter of the Schottky electron gun (~850 nm tip diameter, 160 kV accelerating voltage) with UV laser pulses (257 nm). For the experiments in Fig. 3, the energy spread of the electron pulses is adjusted by varying the UV laser fluence. With increasing fluence, a larger number of electrons is extracted, which increases the energy spread due to space charge interactions occurring in the electron pulse.[43] Electron energy loss spectra are recorded with an in-column Omega-type energy filter. The width σ of the boundary of a nanoparticle is measured by calculating a 26.5 nm wide intensity profile $I(x)$ across the particle boundary and fitting it with the function $I(x) = a\left(1 + \mathrm{erf}\left(\frac{x-x_0}{\sigma\sqrt{2}}\right)\right)$, where $\mathrm{erf}()$ is the error function, and a, x_0, and σ are fit parameters.

Figure 1 illustrates that the outline of a nanoparticle blurs when the electron and laser pulse overlap in time, which provides a straightforward approach for determining time zero. Figure 1a displays

micrographs of a gold nanoparticle (340 nm diameter) on multilayer graphene under illumination with femtosecond laser pulses (22 mJ/cm^2). The particle outline appears crisp when the electron pulse precedes the pump laser pulse by more than 1 ps ($t < t_0$, top panel), but blurs at time zero ($t = t_0$, bottom panel). Figure 1b reveals that this effect is only present when the electron and laser pulse overlap in time. The width of the particle boundary (blue dots) reaches a maximum at time zero, where it almost doubles. The temporal evolution of the width is reasonably well described by a Gaussian fit (red curve, 460 fs FWHM). It is centered at -7±9 fs with respect to the time zero obtained from a measurement using the PINEM effect that is illustrated in Fig. 1c,d. Figure 1c displays the evolution of the electron energy loss spectrum of the same particle as a function of pump-probe delay. At the high laser intensity used in our experiment, the energy spread increases from 3.2 eV to over 20 eV when the electron and laser pulse overlap in time, while the intensity of the zero-loss peak drops to less than 40 %, as shown in Fig. 1d. A Gaussian fit is then used to find time zero (red curve, 620 fs FWHM, centered at 0±1 fs). We conclude that the time zero obtained from monitoring the width of the particle outline agrees closely with that from a PINEM experiment.

Figure 2a provides a hint as to the underlying mechanism of the blurring, revealing that it is most pronounced in the direction of the laser polarization. Whereas the particle boundary shows a uniform width of about 2 nm when the electron and laser pulse do not overlap in time ($t \neq t_0$, blue dots, the solid curve provides a guide to the eye), the blurring at time zero is highly anisotropic ($t = t_0$, red dots). The width of the particle boundary increases to 6 nm in the horizontal direction, while it barely changes in the vertical. The angular dependence of the blurring closely resembles that of the dipolar near fields of the particle, which are revealed in Fig. 2b by an energy gain-filtered micrograph recorded at time zero.[12,16,35,44] We note that when we rotate the laser polarization (double-headed arrow in Fig. 2b), the angular dependence of the blurring rotates accordingly. This suggests that the blurring results from electrons that interact with the near fields of the particle. Since such electrons acquire a large energy spread through the PINEM effect, we propose that the blurring is a consequence of the chromatic aberration of the imaging system.

We verify this hypothesis by demonstrating that the amount of image blurring observed is consistent with the energy spread that the electrons acquire through the PINEM interaction. To this end, we

measure the width of the outline of a nanoparticle in the absence of laser irradiation as a function of energy spread. Figure 3a,b shows that the chromatic aberration blurs the image of a gold nanoparticle (without laser irradiation) when we increase the energy spread of the electron pulses from 6.6 eV (Fig. 3a) to 28.9 eV (Fig. 3b). The corresponding energy loss spectra are shown below the micrographs. Figure 3c reveals that the average width of the particle outline (blue dots) increases by 0.88 nm per 10 eV energy spread, as determined from a linear fit (blue line). The data points highlighted with blue and green circles correspond to the micrographs in Fig. 3a and b, respectively.

When the energy spread of the electrons is increased through the PINEM interaction, the width of the particle outline increases by a similar amount. The red diamonds in Fig. 3c indicate the average boundary width of the particle in the experiment of Fig. 1 as a function of the energy spread that is observed at a given time delay. The data point highlighted with an orange circle corresponds to the micrograph recorded at time zero (Fig. 1a, $t = t_0$), with the corresponding energy loss spectrum in Fig. 3d exhibiting an energy spread of 20.2 eV FWHM. A linear fit of the data (red line) shows that the boundary width increases by 1.1 nm per 10 eV energy spread, in good agreement with the value obtained above. This supports our conclusion that the blurring of the particle boundary at time zero is caused by the large energy spread that the electrons acquire that traverse the near fields of the particle.

We note that the two linear fits predict a different width of the particle boundary at zero energy spread, which is likely the case because both experiments were performed with different nanoparticles and under different imaging conditions. The difference in slope between both data sets likely arises from the fact that the energy spread acquired through the PINEM interaction strongly depends on the local field intensity. The reported energy spread represents an average over regions of different field strength and includes electrons that pass at a large distance from the particle and thus do not gain or lose energy. Our measurement therefore underestimates the energy spread of the electrons close to the particle boundary, which are responsible for the observed blurring and which experience the highest fields. This causes the boundary width to increase more rapidly as a function of the measured energy spread. Finally, we note that at the high laser intensity in our experiment, the nanoparticles undergo ionization.[45] It is however unlikely that the transient electric fields of the emitted electrons can explain the blurring of the particle outline since these fields are known to persist for tens of picoseconds,[26,30]

whereas in our experiment, the blurring can only be observed when the laser and electron pulse overlap in time. Another small contribution to the blurring may arise from the transverse deflection of the electrons in the time-varying near fields,[46] which couples to the spherical aberration.

We have presented a straightforward approach for determining time zero in an ultrafast transmission electron microscope that does not require an energy filter and can therefore find application in most instruments. It relies on the blurring of the outline of a nanoparticle at time zero, an effect that is only present when the electron and laser pulse overlap in time and therefore allows for an accurate measurement. We have shown that this blurring arises from the PINEM effect, which causes electrons that interact with the near fields of a nanoparticle to acquire a large energy spread. Because of the chromatic aberration of the imaging system, these electrons blur the outline of the particle. It should be noted that this effect limits the spatial resolution that can be obtained at time zero, unless of course the chromatic aberration can be corrected. A similar issue arises when the interaction with a time-varying field is employed to compress the electron pulses.[47–52] The blurring of the particle outline at time zero can also be used to visualize the near fields on its surface without using an energy filter and can thus serve as a poor man's PINEM experiment (Fig. 2). Moreover, from the orientation of the dipolar near fields of spherical nanoparticle (Fig. 2a), the laser polarization can easily be determined *in situ*. Finally, our method also provides an estimate of the instrument response (Fig. 1), which is otherwise more difficult to obtain without an energy filter. In the limit of small laser pulse energies, this estimate approaches the actual value.

The data that support the findings of this study are available from the corresponding author upon reasonable request.

The authors declare no competing financial interests.

This work was supported by the Swiss National Science Foundation Grant PP00P2_163681.

Figure 1. Blurring of the boundary of a nanoparticle at time zero. (a) Micrographs of a gold nanoparticle under laser irradiation recorded with electron pulses. The outline of the particle appears crisp when the electron pulse precedes the pump laser pulse by 1 ps, ($t < t_0$, top panels), but blurs when both overlap in time ($t = t_0$, bottom panels). Scale bar, 100 nm. **(b)** Average width of the particle boundary as a function of the pump-probe delay. A Gaussian fit (red line) yields an estimate of the instrument response of 460 fs. **(c)** Temporal evolution of the electron energy loss spectrum of the gold nanoparticle. The spectrum broadens around time zero due to the PINEM effect.[12,35] **(d)** Intensity of the zero-loss peak in (c) as a function of pump-probe delay (5 eV integration window). The maximum drop in intensity, which marks time zero, coincides with the maximum blurring of the particle boundary in (b). A Gaussian fit (red line) yields a FWHM of 620 fs, overestimating the instrument response because of the high laser intensity used in the experiment.

Figure 2. Angular dependence of the boundary blurring at time zero. (a) Angular dependence of the width of the nanoparticle boundary in Fig. 1 when the electron and laser pulse overlap in time ($t = t_0$, red) and when they do not ($t \neq t_0$, blue). The solid lines represent splines of the data. **(b)** Energy gain-filtered image of the same nanoparticle recorded with the laser and electron pulse overlapping in time. The dipolar near fields of the particle are evident, which are aligned with the laser polarization direction (double-headed arrow). The angular dependence of the near fields resembles that in (a). Scale bar, 100 nm.

Figure 3. Boundary blurring as a function of electron energy spread. (a,**b)** The outline of a gold nanoparticle blurs when the energy spread of the incident electron pulses is raised from 6.6 eV in (a) to 28.9 eV in (b) (without laser irradiation of the sample). The energy spread is increased by extracting a larger number of electrons per pulse and thus increasing space charge repulsion. Corresponding electron energy loss spectra are shown below the micrographs. Scale bar, 50 nm. **(c)** Width of the particle boundary as a function of FWHM energy spread of the electron pulses. The data points marked with blue dots correspond to the experiment in (a,b), where the energy spread is induced through space charge interactions in the incident electron pulses (without laser irradiation of the sample). The data points represented with red diamonds correspond to the experiment in Fig. 1, where the energy spread of the electron pulses is increased through their interaction with the near fields of the nanoparticle at time zero under laser irradiation. The solid lines are linear fits that serve as a guide for the eye. The circled data points correspond to the energy loss spectra shown in (a,b) and (d). (**d**) Electron energy loss spectrum corresponding to the data point marked with an orange circle in (c).

References

(1) Lobastov, V. A.; Srinivasan, R.; Zewail, A. H. Four-Dimensional Ultrafast Electron Microscopy. *Proceedings of the National Academy of Sciences* **2005**, *102* (20), 7069–7073.

(2) Barwick, B.; Park, H. S.; Kwon, O.-H.; Baskin, J. S.; Zewail, A. H. 4D Imaging of Transient Structures and Morphologies in Ultrafast Electron Microscopy. *Science* **2008**, *322* (5905), 1227–1231.

(3) Baskin, J. S.; Park, H. S.; Zewail, A. H. Nanomusical Systems Visualized and Controlled in 4D Electron Microscopy. *Nano Letters* **2011**, *11* (5), 2183–2191.

(4) Lorenz, U. J.; Zewail, A. H. Biomechanics of DNA Structures Visualized by 4D Electron Microscopy. *Proceedings of the National Academy of Sciences* **2013**, *110* (8), 2822–2827.

(5) Cremons, D. R.; Plemmons, D. A.; Flannigan, D. J. Femtosecond Electron Imaging of Defect-Modulated Phonon Dynamics. *Nat Commun* **2016**, *7* (1), 11230.

(6) McKenna, A. J.; Eliason, J. K.; Flannigan, D. J. Spatiotemporal Evolution of Coherent Elastic Strain Waves in a Single MoS_2 Flake. *Nano Lett.* **2017**, *17* (6), 3952–3958.

(7) Lobastov, V. A.; Weissenrieder, J.; Tang, J.; Zewail, A. H. Ultrafast Electron Microscopy (UEM): Four-Dimensional Imaging and Diffraction of Nanostructures during Phase Transitions. *Nano Lett.* **2007**, *7* (9), 2552–2558.

(8) Danz, T.; Domröse, T.; Ropers, C. Ultrafast Nanoimaging of the Order Parameter in a Structural Phase Transition. *Science* **2021**, *371* (6527), 371–374.

(9) Carbone, F.; Barwick, B.; Kwon, O.-H.; Park, H. S.; Spencer Baskin, J.; Zewail, A. H. EELS Femtosecond Resolved in 4D Ultrafast Electron Microscopy. *Chemical Physics Letters* **2009**, *468* (4–6), 107–111.

(10) Park, S. T.; Flannigan, D. J.; Zewail, A. H. Irreversible Chemical Reactions Visualized in Space and Time with 4D Electron Microscopy. *J. Am. Chem. Soc.* **2011**, *133* (6), 1730–1733.

(11) Sinha, S. K.; Khammari, A.; Picher, M.; Roulland, F.; Viart, N.; LaGrange, T.; Banhart, F. Nanosecond Electron Pulses in the Analytical Electron Microscopy of a Fast Irreversible Chemical Reaction. *Nat Commun* **2019**, *10* (1), 3648.

(12) García de Abajo, F. J.; Asenjo-Garcia, A.; Kociak, M. Multiphoton Absorption and Emission by Interaction of Swift Electrons with Evanescent Light Fields. *Nano Lett.* **2010**, *10* (5), 1859–1863.

(13) Feist, A.; Echternkamp, K. E.; Schauss, J.; Yalunin, S. V.; Schäfer, S.; Ropers, C. Quantum Coherent Optical Phase Modulation in an Ultrafast Transmission Electron Microscope. *Nature* **2015**, *521* (7551), 200–203.

(14) Vanacore, G. M.; Madan, I.; Berruto, G.; Wang, K.; Pomarico, E.; Lamb, R. J.; McGrouther, D.; Kaminer, I.; Barwick, B.; García de Abajo, F. J.; Carbone, F. Attosecond Coherent Control of Free-Electron Wave Functions Using Semi-Infinite Light Fields. *Nat Commun* **2018**, *9* (1), 2694.

(15) Reinhardt, O.; Kaminer, I. Theory of Shaping Electron Wavepackets with Light. *ACS Photonics* **2020**, *7* (10), 2859–2870.

(16) Kfir, O.; Lourenço-Martins, H.; Storeck, G.; Sivis, M.; Harvey, T. R.; Kippenberg, T. J.; Feist, A.; Ropers, C. Controlling Free Electrons with Optical Whispering-Gallery Modes. *Nature* **2020**, *582* (7810), 46–49.

(17) Hu, J.; Vanacore, G. M.; Cepellotti, A.; Marzari, N.; Zewail, A. H. Rippling Ultrafast Dynamics of Suspended 2D Monolayers, Graphene. *Proc Natl Acad Sci USA* **2016**, *113* (43), E6555–E6561.

(18) Zahn, D.; Hildebrandt, P.-N.; Vasileiadis, T.; Windsor, Y. W.; Qi, Y.; Seiler, H.; Ernstorfer, R. Anisotropic Nonequilibrium Lattice Dynamics of Black Phosphorus. *Nano Lett.* **2020**, *20* (5), 3728–3733.

(19) Kwon, O.-H.; Barwick, B.; Park, H. S.; Baskin, J. S.; Zewail, A. H. Nanoscale Mechanical Drumming Visualized by 4D Electron Microscopy. *Nano Lett.* **2008**, *8* (11), 3557–3562.

(20) Lahme, S.; Kealhofer, C.; Krausz, F.; Baum, P. Femtosecond Single-Electron Diffraction. *Struct. Dyn.* **2014**, *1* (3), 034303.

(21) Yurtsever, A.; Zewail, A. H. Kikuchi Ultrafast Nanodiffraction in Four-Dimensional Electron Microscopy. *Proceedings of the National Academy of Sciences* **2011**, *108* (8), 3152–3156.

(22) Reisbick, S. A.; Zhang, Y.; Chen, J.; Engen, P. E.; Flannigan, D. J. Coherent Phonon Disruption and Lock-In during a Photoinduced Charge-Density-Wave Phase Transition. *J. Phys. Chem. Lett.* **2021**, *12* (27), 6439–6447.

(23) Schliep, K. B.; Quarterman, P.; Wang, J.-P.; Flannigan, D. J. Picosecond Fresnel Transmission Electron Microscopy. *Appl. Phys. Lett.* **2017**, *110* (22), 222404.

(24) Rubiano da Silva, N.; Möller, M.; Feist, A.; Ulrichs, H.; Ropers, C.; Schäfer, S. Nanoscale Mapping of Ultrafast Magnetization Dynamics with Femtosecond Lorentz Microscopy. *Phys. Rev. X* **2018**, *8* (3), 031052.

(25) Schäfer, S.; Liang, W.; Zewail, A. H. Structural Dynamics and Transient Electric-Field Effects in Ultrafast Electron Diffraction from Surfaces. *Chemical Physics Letters* **2010**, *493* (1–3), 11–18.

(26) Zandi, O.; Sykes, A. E.; Cornelius, R. D.; Alcorn, F. M.; Zerbe, B. S.; Duxbury, P. M.; Reed, B. W.; van der Veen, R. M. Transient Lensing from a Photoemitted Electron Gas Imaged by Ultrafast Electron Microscopy. *Nat Commun* **2020**, *11* (1), 3001.

(27) Scoby, C. M.; Li, R. K.; Musumeci, P. Effect of an Ultrafast Laser Induced Plasma on a Relativistic Electron Beam to Determine Temporal Overlap in Pump–Probe Experiments. *Ultramicroscopy* **2013**, *127*, 14–18.

(28) Manz, S.; Casandruc, A.; Zhang, D.; Zhong, Y.; Loch, R. A.; Marx, A.; Hasegawa, T.; Liu, L. C.; Bayesteh, S.; Delsim-Hashemi, H.; Hoffmann, M.; Felber, M.; Hachmann, M.; Mayet, F.; Hirscht, J.; Keskin, S.; Hada, M.; Epp, S. W.; Flöttmann, K.; Miller, R. J. D. Mapping Atomic Motions with Ultrabright Electrons: Towards Fundamental Limits in Space-Time Resolution. *Faraday Discuss.* **2015**, *177*, 467–491.

(29) Plemmons, D. A.; Flannigan, D. J. Ultrafast Electron Microscopy: Instrument Response from the Single-Electron to High Bunch-Charge Regimes. *Chemical Physics Letters* **2017**, *683*, 186–192.

(30) Chen, L.; Li, R.; Chen, J.; Zhu, P.; Liu, F.; Cao, J.; Sheng, Z.; Zhang, J. Mapping Transient Electric Fields with Picosecond Electron Bunches. *Proc Natl Acad Sci USA* **2015**, *112* (47), 14479–14483.

(31) Hebeisen, C. T.; Ernstorfer, R.; Harb, M.; Dartigalongue, T.; Jordan, R. E.; Dwayne Miller, R. J. Femtosecond Electron Pulse Characterization Using Laser Ponderomotive Scattering. *Opt. Lett.* **2006**, *31* (23), 3517.

(32) Hebeisen, C. T.; Sciaini, G.; Harb, M.; Ernstorfer, R.; Dartigalongue, T.; Kruglik, S. G.; Miller, R. J. D. Grating Enhanced Ponderomotive Scattering for Visualization and Full Characterization of Femtosecond Electron Pulses. *Opt. Express* **2008**, *16* (5), 3334.

(33) Gao, M.; Jean-Ruel, H.; Cooney, R. R.; Stampe, J.; de Jong, M.; Harb, M.; Sciaini, G.; Moriena, G.; Dwayne Miller, R. J. Full Characterization of RF Compressed Femtosecond Electron Pulses Using Ponderomotive Scattering. *Opt. Express* **2012**, *20* (11), 12048.

(34) Gerbig, C.; Senftleben, A.; Morgenstern, S.; Sarpe, C.; Baumert, T. Spatio-Temporal Resolution Studies on a Highly Compact Ultrafast Electron Diffractometer. *New J. Phys.* **2015**, *17* (4), 043050.

(35) Barwick, B.; Flannigan, D. J.; Zewail, A. H. Photon-Induced near-Field Electron Microscopy. *Nature* **2009**, *462* (7275), 902–906.

(36) Park, S. T.; Lin, M.; Zewail, A. H. Photon-Induced near-Field Electron Microscopy (PINEM): Theoretical and Experimental. *New Journal of Physics* **2010**, *12* (12), 123028.

(37) Dahan, R.; Nehemia, S.; Shentcis, M.; Reinhardt, O.; Adiv, Y.; Shi, X.; Be'er, O.; Lynch, M. H.; Kurman, Y.; Wang, K.; Kaminer, I. Resonant Phase-Matching between a Light Wave and a Free-Electron Wavefunction. *Nat. Phys.* **2020**, *16* (11), 1123–1131.

(38) Plemmons, D. A.; Tae Park, S.; Zewail, A. H.; Flannigan, D. J. Characterization of Fast Photoelectron Packets in Weak and Strong Laser Fields in Ultrafast Electron Microscopy. *Ultramicroscopy* **2014**, *146*, 97–102.

(39) Kirchner, F. O.; Gliserin, A.; Krausz, F.; Baum, P. Laser Streaking of Free Electrons at 25 KeV. *Nature Photon* **2014**, *8* (1), 52–57.

(40) Houdellier, F.; Caruso, G. M.; Weber, S.; Kociak, M.; Arbouet, A. Development of a High Brightness Ultrafast Transmission Electron Microscope Based on a Laser-Driven Cold Field Emission Source. *Ultramicroscopy* **2018**, *186*, 128–138.

(41) Feist, A.; Bach, N.; Rubiano da Silva, N.; Danz, T.; Möller, M.; Priebe, K. E.; Domröse, T.; Gatzmann, J. G.; Rost, S.; Schauss, J.; Strauch, S.; Bormann, R.; Sivis, M.; Schäfer, S.; Ropers, C. Ultrafast Transmission Electron Microscopy Using a Laser-Driven Field Emitter: Femtosecond Resolution with a High Coherence Electron Beam. *Ultramicroscopy* **2017**, *176*, 63–73.

(42) Wang, K.; Dahan, R.; Shentcis, M.; Kauffmann, Y.; Ben Hayun, A.; Reinhardt, O.; Tsesses, S.; Kaminer, I. Coherent Interaction between Free Electrons and a Photonic Cavity. *Nature* **2020**, *582* (7810), 50–54.

(43) Olshin, P. K.; Drabbels, M.; Lorenz, U. J. Characterization of a Time-Resolved Electron Microscope with a Schottky Field Emission Gun. *Structural Dynamics* **2020**, *7* (5), 054304.

(44) Yurtsever, A.; Baskin, J. S.; Zewail, A. H. Entangled Nanoparticles: Discovery by Visualization in 4D Electron Microscopy. *Nano Lett.* **2012**, *12* (9), 5027–5032.

(45) Voss, J. M.; Olshin, P. K.; Charbonnier, R.; Drabbels, M.; Lorenz, U. J. *In Situ* Observation of Coulomb Fission of Individual Plasmonic Nanoparticles. *ACS Nano* **2019**, *13* (11), 12445–12451.

(46) Ryabov, A.; Baum, P. Electron Microscopy of Electromagnetic Waveforms. *Science* **2016**, *353* (6297), 374–377.

(47) Kealhofer, C.; Schneider, W.; Ehberger, D.; Ryabov, A.; Krausz, F.; Baum, P. All-Optical Control and Metrology of Electron Pulses. *Science* **2016**, *352* (6284), 429–433.

(48) Morimoto, Y.; Baum, P. Diffraction and Microscopy with Attosecond Electron Pulse Trains. *Nature Phys* **2018**, *14* (3), 252–256.

(49) Priebe, K. E.; Rathje, C.; Yalunin, S. V.; Hohage, T.; Feist, A.; Schäfer, S.; Ropers, C. Attosecond Electron Pulse Trains and Quantum State Reconstruction in Ultrafast Transmission Electron Microscopy. *Nature Photon* **2017**, *11* (12), 793–797.

(50) Gliserin, A.; Walbran, M.; Krausz, F.; Baum, P. Sub-Phonon-Period Compression of Electron Pulses for Atomic Diffraction. *Nat Commun* **2015**, *6* (1), 8723.

(51) Miller, R. J. D. Femtosecond Crystallography with Ultrabright Electrons and X-Rays: Capturing Chemistry in Action. *Science* **2014**, *343* (6175), 1108–1116.

(52) Sun, S.; Sun, X.; Bartles, D.; Wozniak, E.; Williams, J.; Zhang, P.; Ruan, C.-Y. Direct Imaging of Plasma Waves Using Ultrafast Electron Microscopy. *Structural Dynamics* **2020**, *7* (6), 064301.

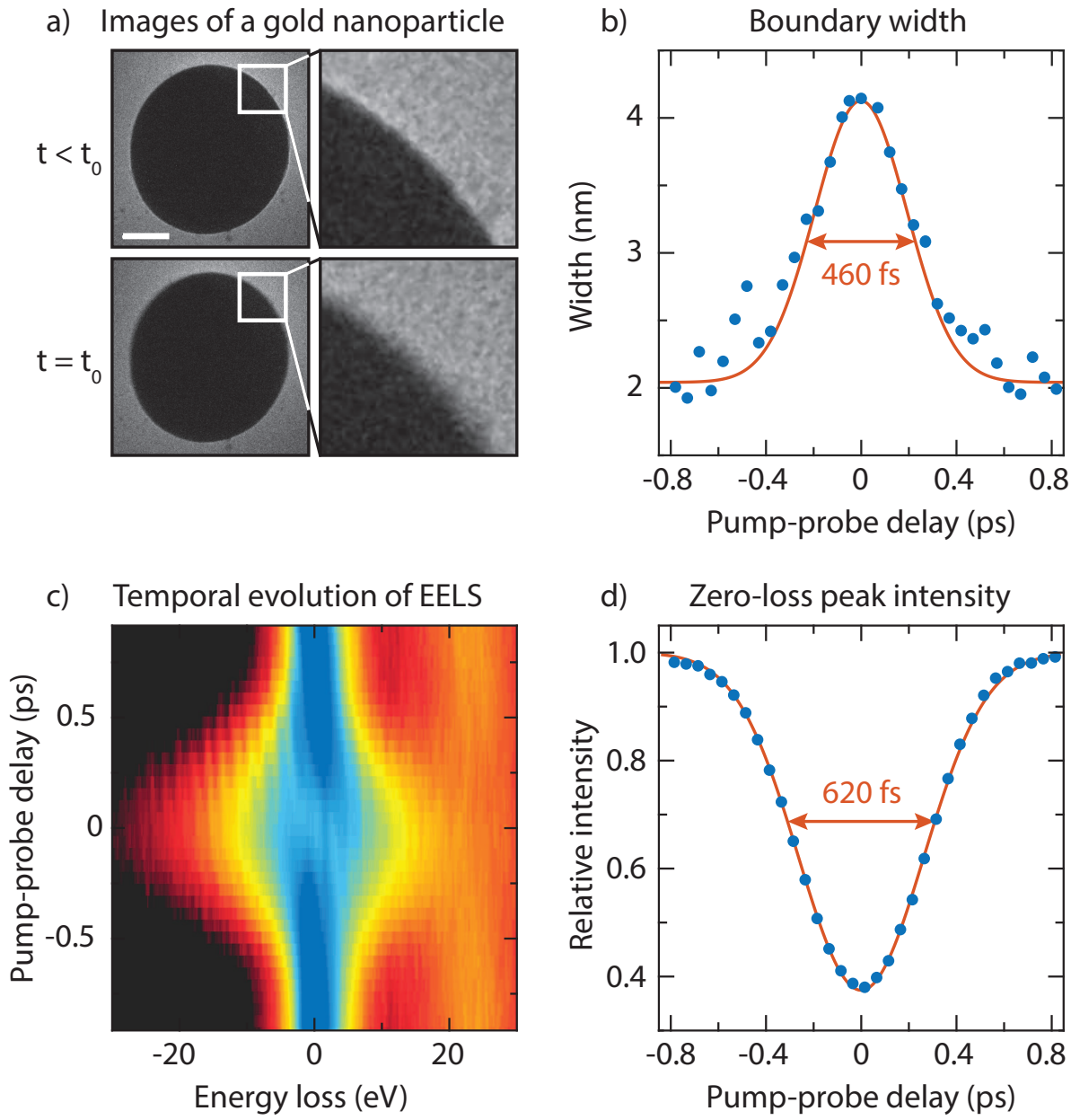

a) Angular dependence of blurring

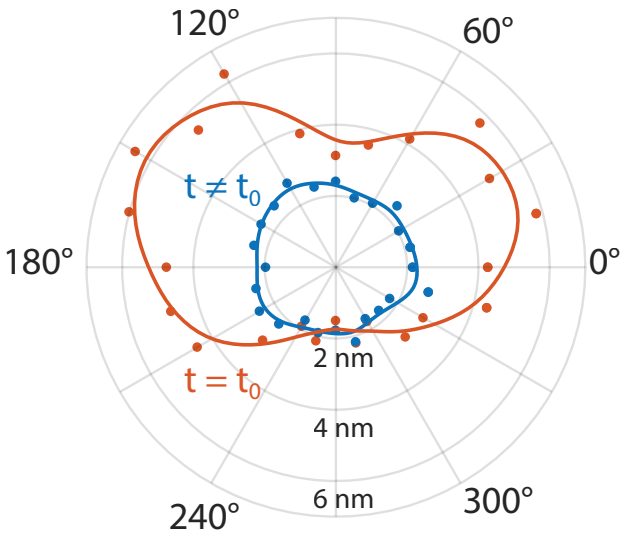

b) Energy gain filtered image